J. Fluid Mech. (1979), *vol.* 90, *part* 4, *pp.* 713–723
Printed in Great Britain

Large amplitude unsteady motion of a flexible slender propulsor

By J. KATZ AND D. WEIHS

Department of Aeronautical Engineering, Technion – Israel Institute of Technology, Haifa

(Received 5 July 1978)

The unsteady large amplitude linearized motion of a flexible slender wing in inviscid incompressible fluid is analysed. This extension to large amplitudes is made by assuming small local angles of incidence during motion along a finite amplitude trajectory. As a specific example, the periodic propulsion produced by a flexible slender wing is analysed for large amplitude harmonic motion with small local angles of attack and results for the available thrust and efficiency are presented.

1. Introduction

The study of the hydromechanics of aquatic-animal propulsion has led to the development of a new branch of unsteady slender-body theory (Lighthill 1970). The first attempts were based on the assumption that the flexible elongated fish body is performing a predetermined periodic motion whose amplitude is small in relation to the body length (Lighthill 1960). An analysis of the swimming of slender fish with dorsal fins was reported by Wu (1971) as part of a general discussion of aquatic propulsion. The influence of fish body thickness and finite fin effects was investigated by Newman & Wu (1973), who transformed the flow equations into time-varying curvilinear co-ordinates attached to the fish backbone as suggested by Lighthill (1960). A more general analysis of the propulsive forces was carried out by Newman (1973).

Large amplitude theory has to be applied in certain cases as the swimming motions of most aquatic animals cannot be approximated by small perturbations about a straight line. A method for solving this problem was suggested by Lighthill (1971), followed by Wu & Yates (1976), who examined the motion of a slender body with circular cross-section performing a predetermined motion.

In the present work the unsteady large amplitude motion of a slender lifting surface is analysed. The effects of passive chordwise flexibility, determined by the time-dependent force balance on the surface, are taken into account here for the first time. The analysis is then applied to the calculation of the propulsive thrust forces and the efficiency of such thrust production. These parameters are of prime importance in the assessment of propulsive units. The present work is a sequel to a similar analysis of large aspect ratio (so-called two-dimensional) airfoils performing oscillatory motions (Katz & Weihs 1978, referred to as I from here on); together these analyses cover most of the range of possible oscillating propulsors.

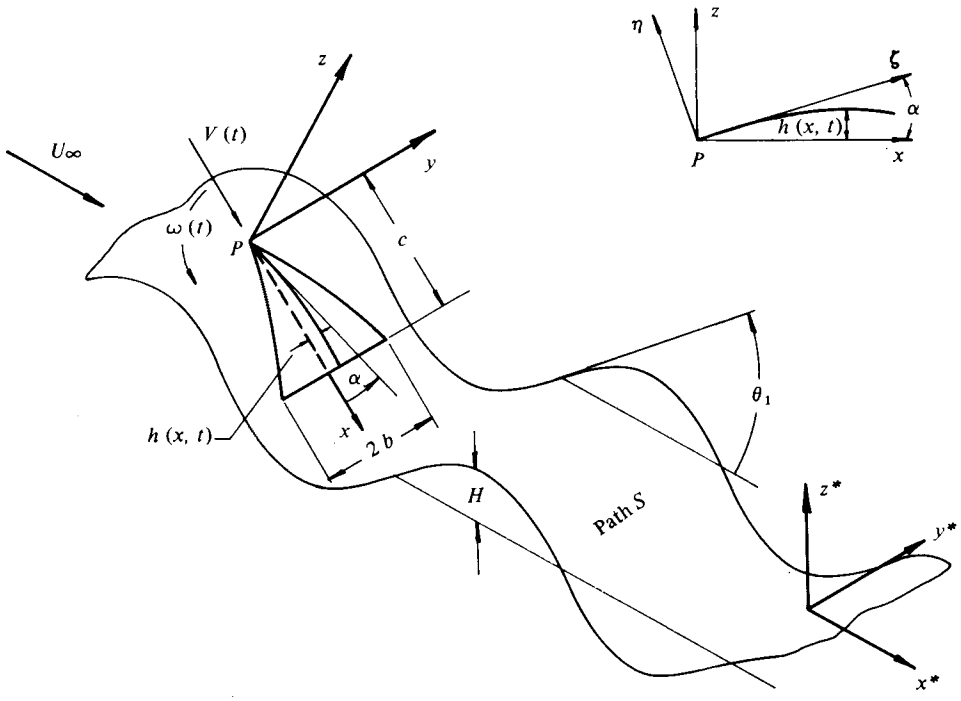

FIGURE 1. Schematic description of the foil motion and the co-ordinate systems used.

2. Analysis

Consider a thin slender fin with aspect ratio smaller than unity moving in a curved path through an inviscid incompressible fluid which is otherwise at rest. The fin is of constant length but is allowed to deform owing to the action of time-dependent hydrodynamic and driving forces and its finite (and assumed given) chordwise flexibility. A given point P (chosen at the front, see figure 1), is forced to follow a predetermined path S. The trajectory S is such that the flow disturbance caused by the foil in each cross-section stays small in a sense described below, and no point of the foil traverses the wake. In addition the displacement of the foil $h(x,t)$ measured in the orthogonal x, y, z co-ordinate system, where the x direction is tangential to the path in the direction of motion, has to be small relative to the local span ($h(x,t)/b(x) \ll 1$). These two statements limit the surface downwash velocity $w(x,t)$ such that:

$$w(x,t)/|V(t)| \ll 1$$

everywhere on the foil, where $V(t)$ is the velocity of point P, i.e. the local angle of attack of each point along the foil is small.

There are two major differences between the solution for the situation described and the analyses existing in the literature (see introduction).

(*a*) The boundary conditions cannot simply be stated at $z^* = 0$, where the star indicates an inertial system (see figure 1) owing to the large excursions allowed between the foil path and any Cartesian inertial co-ordinate.

(*b*) The local deflexions of the chord are calculated from the hydrodynamic forces acting on it, which are themselves dependent on the foil shape.

The method of overcoming the above problems follows that suggested by the authors in a recent analysis of large aspect ratio foil motion (I). First, by applying a transformation to a time-dependent non-inertial system (x, y, z) attached to the foil (see figure 1), the definition of the boundary conditions is obtained.

The boundary-value problem can now be set as the solution of Laplace's equation $\nabla^2\phi = 0$ for the velocity potential, in the non-inertial frame. The condition of no flow through the foil is

$$\left.\frac{\partial\phi}{\partial z}\right|_{z=0,-b<y<+b} = V\frac{\partial h}{\partial x}+\frac{\partial h}{\partial t}+\omega x \equiv W, \tag{1}$$

defining W, where ω is the time-dependent local angular velocity of the y, z plane at given value of x. The disturbance decays far from the scene of motion, so that

$$\lim_{x,\,y,\,z\to\infty} \nabla\phi = 0. \tag{2}$$

The pressures are obtained via Bernoulli's equation for unsteady incompressible flow:

$$\frac{p_\infty - p}{\rho} = (V+\omega z)\frac{\partial\phi}{\partial x}-\omega x\frac{\partial\phi}{\partial z}+\frac{\partial\phi}{\partial t}, \tag{3}$$

where second-order disturbances were neglected relative to quantities containing larger values, such as $V\partial\phi/\partial x$. For the steady case, (3) reduces to the familiar result $p_\infty - p = \rho V\partial\phi/\partial x$. The lateral pressure field is defined by taking cases of zero side-slip only, i.e. the pressure distribution in each cross-flow plane is symmetric about $y = 0$.

Analysis of the deflexions under the assumption that the foil is linearly elastic so that no 'memory' effects have to be taken into account leads (I) to the time-dependent partial differential equation

$$\frac{\partial^2}{\partial\zeta^2}\left[E(\zeta)\frac{\partial^2\eta}{\partial\zeta^2}\right] = \frac{\partial L(\zeta,t)}{\partial\zeta}\cos\alpha. \tag{4}$$

Here ζ and η are defined in an additional Cartesian non-inertial co-ordinate system originating at the point P, where ζ is inclined to the x direction at the angle of incidence α. $E(\zeta)$ is the chordwise rigidity of the foil defined as the product of the local moment of inertia and Young's modulus, while $\partial L/\partial\zeta$ is the variation of the total lift-force distribution on the foil, which is obtained by solving the potential flow field around the wing. The solution of the above elastic equation is obtained by iteration, neglecting the mass of the foil as described in I.

The pressure distribution about a slender, pointed, flexible foil is now found by slender-wing methods with some modifications to allow the inclusion of large amplitude time-dependent motions.

The slenderness assumptions introduced can be written as

$$\frac{\partial}{\partial x} = O\left(\frac{1}{c}\right), \quad \frac{\partial}{\partial y}, \frac{\partial}{\partial z} = O\left(\frac{1}{2b(x)}\right), \quad AR = \frac{2b}{c} \ll 1, \tag{5}$$

furthermore the path curvature R is

$$P = (S'')^{-1}[1+(S')^2]^{\frac{3}{2}}, \tag{6}$$

where $R/c \gg 1$ and the displacement $h(x,t)$ relative to the x,y,z co-ordinate system is limited (see figure 1) to values $h/b \ll 1$.

The variations of the velocity potential in the x direction are therefore smaller than those in the y and x directions ($\partial^2\phi/\partial x^2 \ll \partial^2\phi/\partial y^2, \partial^2\phi/\partial z^2$). Thus, by neglecting the $\partial^2\phi/\partial^2 x$ term in Laplace's equations, we retain the flow in the so-called cross-flow plane, solving

$$\partial^2\phi/\partial y^2 + \partial^2\phi/\partial z^2 = 0 \tag{7}$$

for each plane $x =$ constant, while the boundary conditions remain as stated in (1) and (2).

Following Robinson & Laurmann (1956), we define a complex variable $\lambda = y + iz$ and complex potential $F(\lambda) = \phi + i\psi$, where ψ is the stream function. The boundary conditions for $F(\lambda)$ are

$$w^{\pm}\Big|_{z=0,-b<y<b} = \mathrm{Im}\left|\frac{dF(\lambda)}{d\lambda}\right| = V(t)\frac{\partial h(x,t)}{\partial x} + \frac{\partial h(x,t)}{\partial t} + \omega x \equiv W(x,t), \tag{8}$$

$$\lim_{\lambda\to\infty}[dF(\lambda)/d\lambda] = 0, \tag{9}$$

where the first term of (8) describes the local downwash due to the instantaneous angle of attack, which is the sum of the forced angle of attack and the elastic chord distortion. The last two terms describe the unsteady downwash caused by vertical displacement and rotation. Here the foil span is not allowed to bend under the action of the forces. As a result the downwash W is a function of the chordwise location and time only.

The solution for $F(\lambda)$ in the complex plane is given by Robinson & Laurmann (1956, chap. 3.10) as a function of the spanwise co-ordinate θ, defined as

$$\cos\theta = y/b(x).$$

$F(\lambda)$ can thus be written in the form of an infinite series in θ:

$$F(\lambda) = \phi + i\psi = i\sum_{n=1}^{\infty} a_n[\cos n\theta - i\sin n\theta]. \tag{10}$$

The velocity components are then

$$v^{\pm} = \frac{\partial\phi}{\partial y} = \frac{-1}{b(x)\sin\theta}\sum_{n=1}^{\infty} n a_n \cos n\theta, \tag{11}$$

$$w^{\pm} = \frac{\partial\phi}{\partial z} = \frac{-1}{b(x)\sin\theta}\sum_{n=1}^{\infty} n a_n \sin n\theta, \tag{12}$$

where the values of the coefficients a_n have to be real numbers in order to obtain symmetry of the potential $F(\lambda)$ relative to the z axis. The a_n are calculated by equating the downwash expansion in (12) to its value in the boundary conditions (8):

$$a_n \equiv a_n(x,t) = \frac{-2}{n\pi}\int_0^{\pi} W(x,t)\, b(x)\sin\theta\sin n\theta\, d\theta. \tag{13}$$

Now that the complete solution in any cross-flow plane has been obtained, it can

be applied to finding the chordwise variations in velocity $\partial\phi/\partial x$ by differentiation (as in the steady flow case):

$$u^{\pm} = \frac{\partial\phi}{\partial x} = \sum_{n=1}^{\infty} \frac{\partial a_n}{\partial x} \sin n\theta + \frac{1}{b(x)\tan\theta} \frac{db(x)}{dx} \sum_{n=1}^{\infty} n a_n \cos n\theta, \tag{14}$$

the time-dependent effect being introduced here through the coefficient a_n, which is a function of time also.

The only unknown term left in Bernoulli's equation (3) is $\partial\phi/\partial t$, which is calculated in a similar way to (11)–(14) and is found to be

$$\frac{\partial\phi}{\partial t} = \sum_{n=1}^{\infty} \frac{\partial a_n}{\partial t} \sin n\theta. \tag{15}$$

The terms including the contribution of the angular velocity ω are symmetric with respect to the wing profile and do not contribute to the lift distribution, which is calculated by spanwise integration of the pressure difference Δp:

$$\frac{dL}{dx} = \int_{-b(x)}^{+b(x)} \Delta p \, dy = 2\rho \int_0^{2\pi} \left[\frac{\partial\phi}{\partial t} + V(t)\frac{\partial\phi}{\partial x}\right] b(x) \sin\theta \, d\theta. \tag{16}$$

The integral in (16) is evaluated by substituting (14) and (15) and is found to be

$$\frac{dL}{dx} = \pi\rho \left\{ b(x) \frac{\partial a_1(x,t)}{\partial t} + V(t) \frac{\partial}{\partial x}\left[a_1(x,t)\, b(x)\right] \right\}. \tag{17}$$

In the steady case this expression reduces to $dL/dx = \pi\rho V d[a_1 b(x)]/dx$ which can be further simplified to obtain the well-known result for a constant angle of attack α, where $a_1 = b(x)\, V\alpha$:

$$\frac{dL}{dx} = \pi\rho V^2 \alpha \, db^2(x)/dx. \tag{18}$$

The total lift and couple are then found by integrating (17) over the entire chord length, which is possible only by numerical means for the general unsteady case.

3. Performance calculations for a harmonically oscillating slender propulsor

Here we consider a slender flexible lifting surface of variable span with $b(0) = 0$ which is oscillating in heaving and pitching motion with constant amplitudes H and α_0, respectively. Strictly speaking, b has to be a monotonically increasing function of x so that the wake of each section is 'absorbed' in the flow about following sections. However, regions where $db/dx < 0$ can be considered roughly as if b = constant (Lighthill 1970; Newman & Wu 1973). The instantaneous angles of attack are small, so that assumptions (6) and (7) are valid, and during the cycle there is no appreciable separation, which can cause a different flow pattern around the propulsor.

Assuming that the propulsive fin is attached to a vehicle which is moving in the $-x^*$ direction with speed U_∞ and that the propulsor is performing a heaving and pitching motion with a frequency Ω and phase difference ψ, the path parameters can be written as

$$x^* = -U_\infty t, \quad S = (H/c)\sin\Omega t, \tag{19}$$

$$\alpha = \alpha_1 + \alpha_0 \sin(\Omega t - \psi), \tag{20}$$

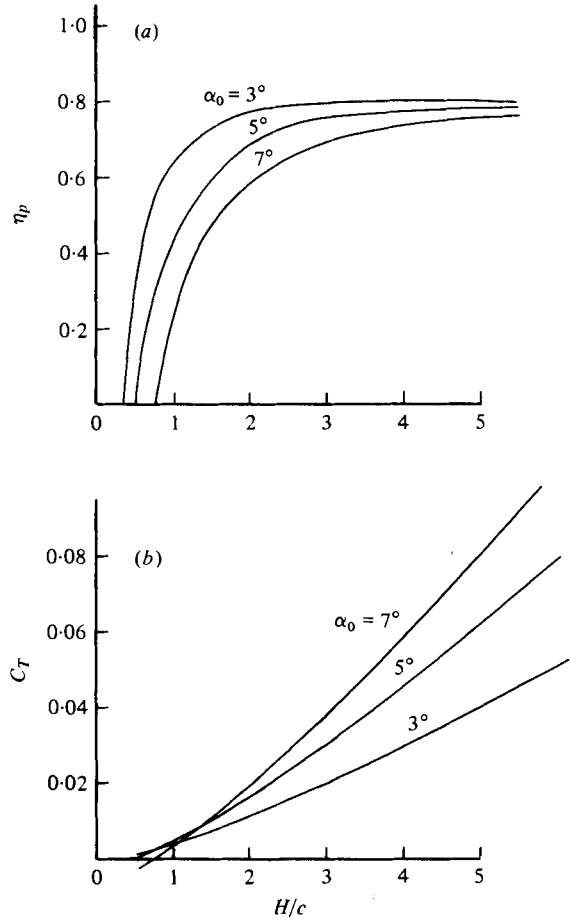

FIGURE 2. The influence of the maximal angle of attack on (*a*) the efficiency and (*b*) the thrust coefficient of a flexible slender fin. $2b/c = 0{\cdot}5$, $U_\infty/c = 10\ \mathrm{s}^{-1}$, $\Omega = \frac{1}{2}\pi$ ($\sigma = 0{\cdot}0785$), $\psi = \frac{1}{2}\pi$.

$$\theta_1 = \tan^{-1}\left[\frac{dx^*}{dt}\Big/\frac{dS(x^*)}{dt}\right], \tag{21}$$

$$\omega = d\theta/dt. \tag{22}$$

The instantaneous forces acting in the x and z directions are calculated by integrating the pressure difference obtained in (16) and (17):

$$\Sigma F_x = -\int_0^c \frac{dL}{dx}\frac{\partial h}{\partial x}dx, \quad \Sigma F_z = \int_0^c \frac{dL}{dx}dx, \tag{23), (24}$$

$$\Sigma M_y = \int_0^c \frac{dL}{dx}x\,dx. \tag{25}$$

The effects of leading-edge suction (Wu 1971) are omitted in (23) as this effect is basically much smaller for slender fins, where the leading edges are almost perpendicular to the direction of motion ($db/dx \ll 1$), so that the component in the thrust direction is only a small part of the total suction. This component is further reduced by the fact that in large amplitude motion the suction vectors are deflected from the direction of advance during most of the cycle, while the thrust is greatly enhanced

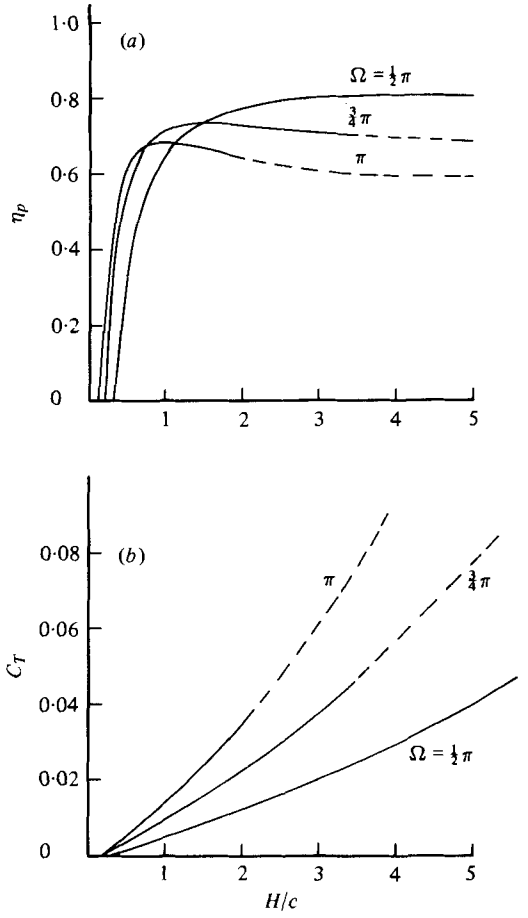

FIGURE 3. The influence of the frequency on (*a*) the efficiency and (*b*) the thrust coefficient of a slender fin. $2b/c = 0{\cdot}5$, $U_\infty/c = 10\ \mathrm{s}^{-1}$, $\psi = \frac{1}{2}\pi$, $\alpha_0 = 3°$.

(see figures 2 and 3, for example). The omission of the small leading-edge suction is, in any case, a conservative assumption as inclusion of this effect will increase the thrust, and therefore also the efficiency.

The thrust coefficient C_T and the propulsive efficiency η_p are defined as

$$C_T = \frac{2}{\rho U_\infty 2c}\frac{1}{\tau}\int_0^\tau (\Sigma F_x \cos\theta_1 - \Sigma F_z \sin\theta_1)\,dt, \tag{26}$$

$$\eta_p = \frac{\int_0^\tau \left\{(\Sigma F_x \cos\theta_1 - \Sigma F_z \sin\theta_1)\frac{dx^*}{dt}\right\} dt}{\int_0^\tau \left\{(\Sigma F_x \sin\theta_1 + \Sigma F_z \cos\theta_1)\frac{dz}{dt} + M_y \frac{d(\alpha+\theta)}{dt}\right\} dt}, \tag{27}$$

where τ is a whole number of periods of oscillation.

The variation of C_T and η_p as a function of the amplitude ratio H/c, the maximum angle of attack α_0 and the frequency is given in figures 2 and 3. In this case the propulsor has a rigid chord in order to emphasize the advantages of large amplitude propulsion, which is both efficient and provides high propulsive thrust above $H/c > 3$.

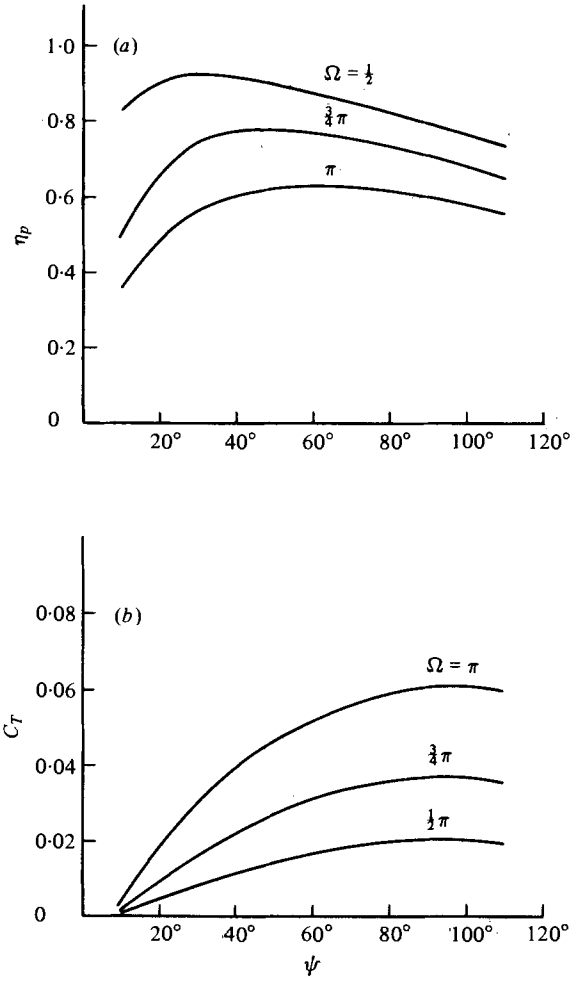

FIGURE 4. The influence of the phase difference ψ between heaving and pitching on (*a*) the efficiency and (*b*) the thrust coefficient. $2b/c = 0{\cdot}5$, $U_\infty/c = 10\ \mathrm{s}^{-1}$, $\alpha_0 = 3°$, $H/c = 3$.

Results of the type appearing in figures 2 and 3 for a two-dimensional foil of large aspect ratio were reported by Chopra (1976) and in I.

The dashed lines in figure 3 represent regions where the local downwash on the wing reaches higher values than are permitted by linear theory (strong leading-edge vortices are then expected). This usually occurs after the extremal values of the sinusoidal motion and can strongly affect the efficiencies, thus invalidating further calculations.

Figures 2 and 5 show that the thrust and efficiency increase when the amplitude H/c grows. However, if the path curvature is increased (e.g. if the frequency Ω grows while H/c = constant > 2 in figure 3), the efficiency will decrease. This is due to the extra effort invested in the foil pitching at the extremes of the sinusoidal motion, with no additional thrust component. For the same reason the efficiency will increase when the phase difference ψ between the heaving and pitching motions is changed as indicated in figure 4. The thrust coefficient is highest when the phase difference is

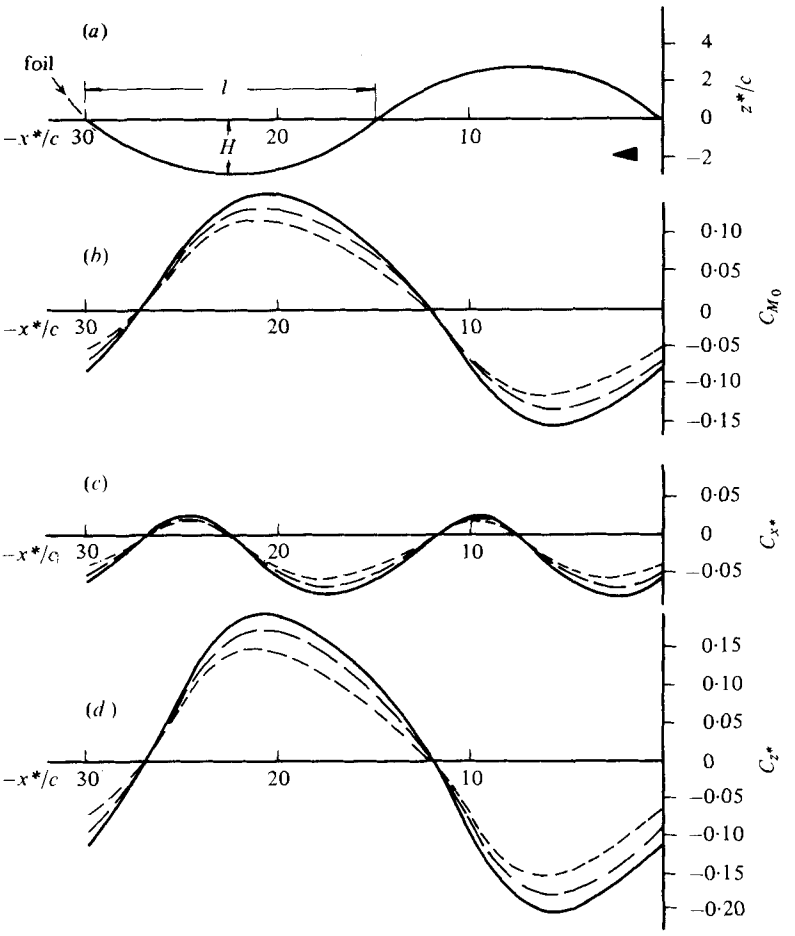

FIGURE 5. Variation of couples and forces during periodic motion of a flexible fin. —— $E/T_{av}c^2 = \infty$; — —, $E/T_{av}c^2 = 131$; – – – –, $E/T_{av}c^2 = 52$. $2b/c = 0{\cdot}5$, $U_\infty/c = 10\ \mathrm{s}^{-1}$, $\Omega = \frac{2}{3}\pi$, $\psi = \frac{1}{2}\pi$, $H/c = 3$.

close to 90°. This result is reminiscent of large aspect ratio results (I). It has been observed in the swimming of fish with both large and small aspect ratio propulsors and was also found experimentally by Scherer (1968), who tested a rectangular propulsor of aspect ratio 3. This leads to the conclusion that a phase difference of $\sim 90°$ is probably optimal for all oscillating propulsors.

The effect of a constant chordwise flexibility distribution $E(\zeta) =$ constant on the variation of moments and forces during a propulsive cycle is illustrated in figure 5. The solid line stands for the performance of a rigid propulsor while the other lines show the results for flexible ones. The parameter $E/(T_{av}c^2)$ describes the normalized deflexion of the propulsor chord and T_{av} is the average thrust of a rigid propulsor performing the same periodic motion. It is clear from figure 5 that the flexibility reduces the magnitude of the forces but does not appreciably change their time dependence.

The variation of the thrust coefficient C_T and efficiency η_p with increasing flexibility parameter $E/(T_{av}c^2)$ is displayed in figure 6. There is a considerable gain in efficiency up to $E/(T_{av}c^2) \simeq 10$, while the loss in thrust is small. This phenomenon

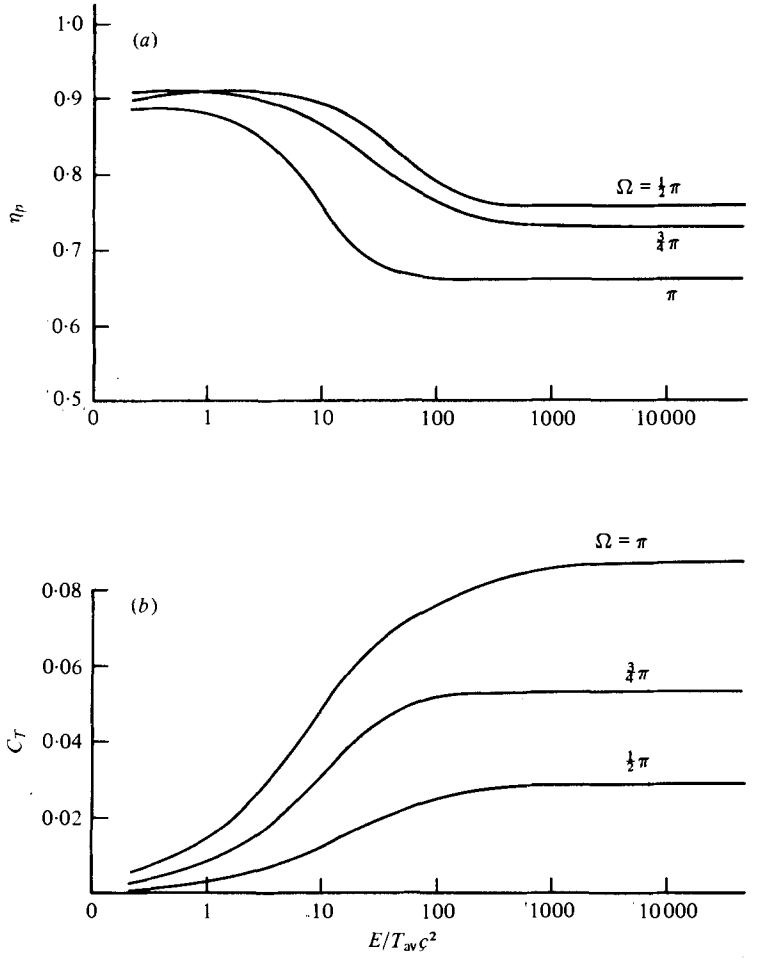

FIGURE 6. The influence of flexibility on (*a*) the efficiency and (*b*) the thrust coefficient of a slender fin. $2b/c = 0{\cdot}5$, $U_\infty/c = 10\ \mathrm{s}^{-1}$, $\phi = \frac{1}{2}\pi$, $\alpha = 5°$, $H/c = 3$.

was realized qualitatively by Picken & Crowe (1974), who compared the performance of various flexible swim fins experimentally. For very flexible swim fins the thrust is rather small and not sufficient for propulsive purposes.

REFERENCES

CHOPRA, M. G. 1976 Large amplitude lunate-tail theory of fish locomotion. *J. Fluid Mech.* **74**, 161–182.

KATZ, J. & WEIHS, D. 1978 Hydrodynamic propulsion by large amplitude oscillation of an airfoil with chordwise flexibility. *J. Fluid Mech.* **88**, 485–497.

LIGHTHILL, M. J. 1960 Note on the swimming of slender fish. *J. Fluid Mech.* **9**, 305–317.

LIGHTHILL, M. J. 1970 Aquatic animal propulsion of high hydromechanical efficiency. *J. Fluid Mech.* **44**, 265–301.

LIGHTHILL, M. J. 1971 Large amplitude elongated body theory of fish locomotion. *Proc. Roy. Soc.* B **179**, 125–138.

NEWMAN, J. N. 1973 The force on a slender fish-like body. *J. Fluid Mech.* **58**, 689–702.

NEWMAN, J. N. & WU, T. Y. 1973 A generalized slender-body theory for fish-like forms. *J. Fluid Mech.* **57**, 675–693.

PICKEN, J. & CROWE, C. T. 1974 *Ocean Engng* **2**, 251–258.

ROBINSON, A. & LAURMANN, J. A. 1956 *Wing Theory* chap 3. Cambridge University Press.

SCHERER, J. O. 1968 Experimental and theoretical investigation of large amplitude oscillating foil propulsion systems. *Hydronautics Tech. Rep.* no. 662–1.

WU, T. Y. 1971 Hydromechanics of swimming propulsion. Parts 2 and 3. *J. Fluid Mech.* **46**, 521–544, 545–568.

WU, T. Y. & YATES, G. T. 1976 *Proc. 11th ONR Symp. Naval Hydrodyn., London*, pp. 517–528.